An Effective Approach to Deembed the Complex Propagation Constant of Half-Mode SIW and Its Application

Zheng Liu, *Student Member, IEEE*, Lei Zhu, *Fellow, IEEE*, Gaobiao Xiao, *Member, IEEE*, and Qiong Sen Wu

***Abstract*— In this paper, a numerical short-open calibration (SOC) method is presented to numerically deembed the complex propagation constant of half-mode substrate integrated waveguide (HMSIW). After three distinctive equivalent circuit networks are described for SOC deembedding procedures, the propagation characteristics of HMSIW can be extracted. The numerical stability and convergence are illustrated. Two examples designed with the application of our method are given. An HMSIW leaky wave antenna is designed, fabricated, and measured. The radiation pattern calculated from the deembedded complex propagation constant is well verified by the simulated and measured ones. The scattering parameters of two classes of single microstrip-to-SIW transitions are extracted and they are used to validate the numerically deembedded complex propagation constant of SIW.**

***Index Terms*— Leaky wave antenna, propagation constant, radiation pattern, short-open calibration (SOC), transition.**

I. Introduction

MODERN communication systems are usually composed of various kinds of microwave active and passive components, whose miniaturization and integration are one of the research topics in recent years. Substrate integrated waveguide (SIW) and half-mode SIW (HMSIW) are widely considered as promising candidates for microwave and millimeter-wave integrated circuits due to their compact size, low cost, and easy integration with other planar circuits [1], [2]. Numerical papers have been published to develop the principle characteristics of SIW or HMSIW and the applications, such as filters [3]–[9], couplers [10], [11], antennas [12]–[15], and so on. Meanwhile, various commercial electromagnetic (EM) softwares have been developed to allow us to simulate the overall layout of an SIW or HMSIW circuit block. As one drawback, these simulators can only calculate the resultant network parameters at specified external locations along the feeding lines and they cannot accurately and directly calculate the propagation characteristics of SIW or HMSIW due to the high-order mode effects and port discontinuities in EM modeling [16], [17]. However, the complex propagation constants of SIW and HMSIW are the critical parameters, which are highly demanded in circuit and antennas design, such as predicting the radiation pattern of leaky wave antennas [12]–[15] and analyzing the crosstalk in SIW high-speed interconnect circuits [18], [19].

To circumvent this problem, a few numerical methods, such as method of auxiliary sources [20], finite difference time domain [21], boundary integral-resonant mode expansion [22], and so on, were proposed to accurately calculate the propagation characteristics of SIW or HMSIW. However, they usually require tedious procedure in programming. Some closed-form formulas to calculate the phase constants of SIW and HMSIW were derived in [22]–[24], while the attenuation constant cannot be calculated by them, which has limited their wide application in some situations. On the other hand, various calibration techniques in experiment and simulation are considered as an effective methodology to remove the port discontinuities out of the device under test (DUT) or model. Many papers have been published so far to investigate and report the deembedded parameters for various microstrip-line discontinuities and periodically varied guided-wave structures in [25]–[30].

The short-open numerical calibration (SOC) technique proposed in [25] was initially realized to deembed the microstrip-line discontinuities in the 2.5-D method of moment (MoM) algorithm, and it is extended in this paper to numerically deembed the complex propagation constants of SIW and HMSIW in the 3-D finite-element method algorithm. The equivalent circuit networks and basic principle of this simplified numerical calibration method are given. In addition to verify the deembedded results as compared with those from the numerical multiline method and empirical formulas, numerical convergence and accuracy of this method are demonstrated and confirmed. Finally, two examples are given to verify the accuracy of our method. One is an HMSIW

Manuscript received May 18, 2015; revised August 27, 2015; accepted October 25, 2015. Date of publication November 24, 2015; date of current version January 15, 2016. This work was supported in part by the Science and Technology Development Fund Research Project under Grant 051/2014/A1 through the Macao Science and Technology Development Fund and in part by the Multi-Year Research through the University of Macau, Macau, China, under Grant MYRG2014-00079-FST. Recommended for publication by Associate Editor T.-L. Wu upon evaluation of reviewers' comments.

Z. Liu is with the Key Laboratory of Ministry of Education of Design and Electromagnetic Compatibility of High Speed Electronic Systems, Shanghai Jiao Tong University, Shanghai 200240, China, and also with the Department of Electrical and Computer Engineering, University of Macau, Macau 999078, China (e-mail: lzheng_2012@sjtu.edu.cn).

L. Zhu and Q. S. Wu are with the Department of Electrical and Computer Engineering, Faculty of Science and Technology, University of Macau, Macau 999078, China (e-mail: leizhu@umac.mo; wuqiongsen@gmail.com).

G. Xiao is with the Key Laboratory of Ministry of Education of Design and Electromagnetic Compatibility of High Speed Electronic Systems, Shanghai Jiao Tong University, Shanghai 200240, China (e-mail: gaobiaoxiao@sjtu.edu.cn).

Color versions of one or more of the figures in this paper are available online at http://ieeexplore.ieee.org.

Digital Object Identifier 10.1109/TCPMT.2015.2496629

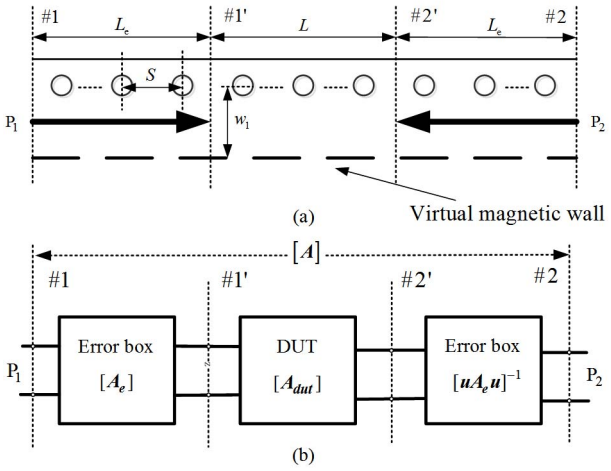

Fig. 1. (a) Schematic for EM modeling of HMSIW. (b) Equivalent circuit representation for SOC deembedding procedure.

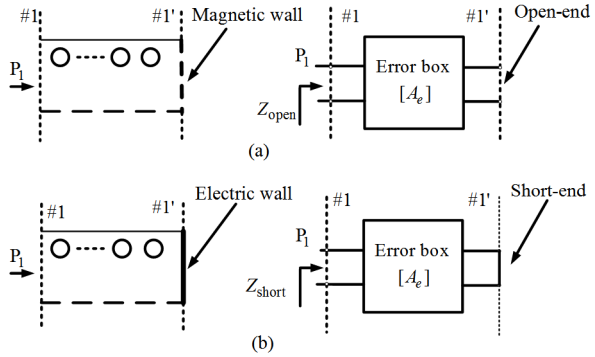

Fig. 2. Two calibration standards in SOC, namely, open- and short-end circuits, by terminating the HMSIW feeders with (a) magnetic wall and (b) electric wall.

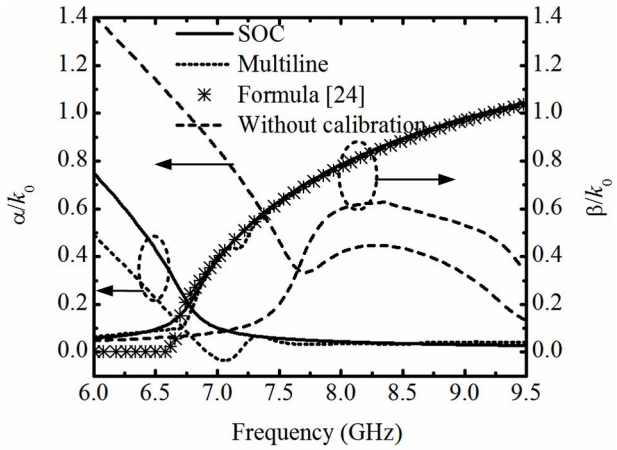

Fig. 3. Calculated normalized complex propagation constants of HMSIW. k_0 is the free-space phase constant. $w_1 = 6.3$ mm, $S = 1.2$ mm, $L_e = 10.8$ mm, $L = 6$ mm, and via's diameter of 0.7 mm.

leaky wave antenna. The radiation pattern calculated from the SOC-derived complex propagation constant is found in good agreement with the simulated and measured ones. The other is to calculate the scattering parameters of two classes of single microstrip-to-SIW transitions by using the numerically deembedded complex propagation constant of SIW with our proposed method.

II. SOC Deembedding Technique

Fig. 1(a) shows a general schematic for EM modeling of an HMSIW with finite length (L). The entire layout in Fig. 1 is classified into three distinctive sections, i.e., two feeding HMSIW sections in the regions of $\#1-\#1'$ and $\#2-\#2'$, and core HMSIW section $\#1'$ and $\#2'$. P_1 and P_2 indicate the port locations where the external field excitations are introduced, whereas $\#1'$ and $\#2'$ stand for the reference planes, to which only the dominant mode can reach from $\#1'$ to $\#2'$.

Fig. 1(b) shows its equivalent circuit representation with three distinctive sections. The middle HMSIW section between $\#1'$ and $\#2'$ is referred as to a DUT, and its ABCD matrix, denoted as $[\boldsymbol{A}_{\rm dut}]$, needs to be deembedded. The feeding line blocks are named the error boxes and their ABCD matrices are expressed as $[\boldsymbol{A}_e]$ and $[\boldsymbol{uA}_e\boldsymbol{u}]^{-1}$, respectively. Thus, $[\boldsymbol{A}_{\rm dut}]$ can be simply derived if $[\boldsymbol{A}_e]$ is determined [25]

$$[A_{\rm dut}] = [A_e]^{-1}\ [A]\ [uA_eu] \tag{1}$$

where $[\boldsymbol{A}] = [e_1, e_2; e_3, e_4]$, $[\boldsymbol{A}_e] = [a_e, b_e; c_e, d_e]$, and $[\boldsymbol{u}] = [1, 0;\ 0, -1]$.

The matrix $[\boldsymbol{A}]$ in (1) represents the overall ABCD matrix and it can be obtained by simulating this entire HMSIW layout in Fig. 1(a). Meanwhile, the feeding line blocks in Fig. 2, terminated with electric and magnetic walls, can be simulated by EM software, thus their input impedances, $Z_{\rm open}$ and $Z_{\rm short}$, at the source plane #1 can be obtained accordingly. Considering that the error box is a reciprocal network, the complex propagation constant of DUT can be explicitly calculated in terms of the above-derived $[\boldsymbol{A}]$, $Z_{\rm open}$ and $Z_{\rm short}$ as follows:

$$\cosh(\gamma L) = \frac{(Z_{\rm open} + Z_{\rm short})(e_1 + e_4) - 2Z_{\rm open}Z_{\rm short}e_3 - 2e_2}{2(Z_{\rm open} - Z_{\rm short})} \tag{2}$$

where γ is the complex propagation constant of HMSIW, including the phase and attenuation constants, β and α.

Note that in [25], the matrix $[\boldsymbol{A}_{\rm e}]$ needs to be obtained first so that the four independent equations must be established. To solve this matrix, the port voltages and currents are required, which had been obtained with the MoM in [25]. However, in this paper, only the two elements, i.e., a_e and d_e, are required to calculate the concerned complex propagation constant, γ. As a result, only the two input impedances of two one-port error boxes with short- and open-circuited ends are needed in the 3-D full-wave software, thus simplifying our deembedding implementation.

The calculated normalized complex propagation constants of the HMSIW with and without carrying out SOC deembedding procedures are shown in Fig. 3. They are plotted together with the results from well-known multiline calibration method [17], [31] and closed-form formula [24]. It is clear that the normalized propagation constant from the SOC in Fig. 3

is exactly the same as that from the multiline method and closed-form formula (note that the attenuation constant cannot be calculated with closed-form formula), whereas the direct EM-derived results without calibration deviate from the cutoff frequency significantly. After studying the latter case, we can figure out that this numerical deviation or instability is mainly attributed by approximate effect of the introduced fields at the port terminals, P_1 and P_2, i.e., that is referred as to the port discontinuities in EM modeling as emphasized in [16], [17], and [25]. Compared with the closed-form formulas [22]–[24], our proposed deembedding method can not only calculate the phase constant, β, but also can derive its attenuation constant, α. The numerical stability and convergence of the multiline line method are directly related to the lengths of two SIWs, which should be selected carefully. Based on our experience, when their lengths are close to each other, weak convergence and small perturbation of obtained complex propagation constant may be observed, especially in the cutoff frequency. On the contrary, our proposed method has good numerical stability and convergence, which will be validated in the following section III.

III. Numerical Stability and Convergence

Using the above-described SOC method, the two identical error boxes, including the port discontinuities and high-order mode effects, can be numerically evaluated. As the lengths of two feeding lines are enlarged beyond a certain value [25], [26], all the high-order modes as evanescent waves eventually disappear at the reference planes. The deembedded ABCD matrix of the DUT, i.e., $[\boldsymbol{A}_{\rm dut}]$, corresponds to a finite-length HMSIW with only its dominant propagating mode, and thus the calculated complex propagation constant gradually converges to a fixed value.

Fig. 4(a) and (b) shows the calculated normalized phase constants and attenuation constants of the DUT, respectively, with respect to different feeding-line lengths. As the via-to-via unit number, n_e, exceeds 3 or feeding-line length increases to three times via-to-via spacing S, i.e., $L_e = 3S$, the calculated complex propagation constants numerically converge to a fixed graph, as shown in Fig. 4.

When the port discontinuities have been included in the error boxes, the calculated normalized phase constant and attenuation constant should converge to a fixed value, respectively, which is independent of the length of DUT in Fig. 1(a), i.e., L. Fig. 5 shows the normalized complex propagation constants under the number of vias, $n = 2$, 3, 5, and 7. We can see that the results agree well with each other under different values of n and have good numerical stability.

Figs. 4 and 5 show that the length of the error box is a key factor which can affect the numerical stability. Compared with the well-known multiline method, our method has simplified the problem of selection of lines' length and can avoid the numerical stability effectively.

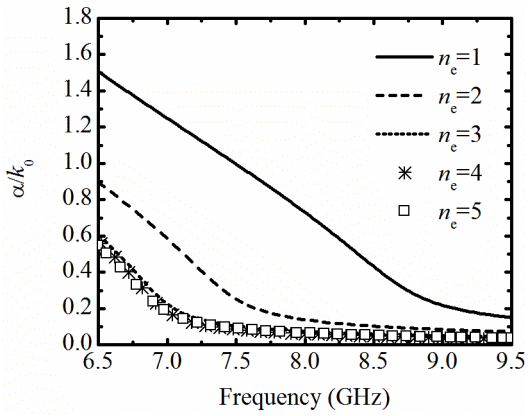

(a)

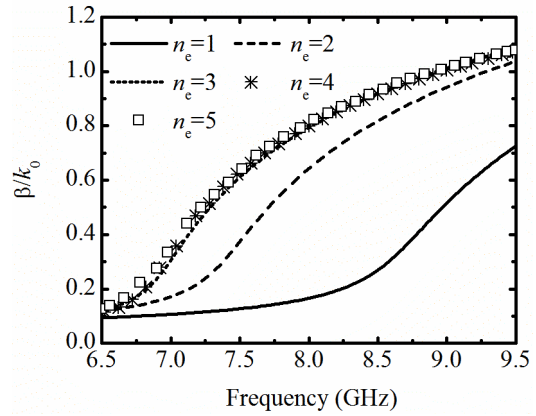

(b)

Fig. 4. Numerical convergence on deembedded complex propagation constants with respect to different HMSIW feeding lengths, $L_e = n_e S$. n_e: vias' number. S: via-to-via spacing. $L = 3S$, $w_1 = 6.3$ mm, and $S = 1.2$ mm. The via's diameter is 0.7 mm. (a) Normalized attenuation constants. (b) Normalized phase constants.

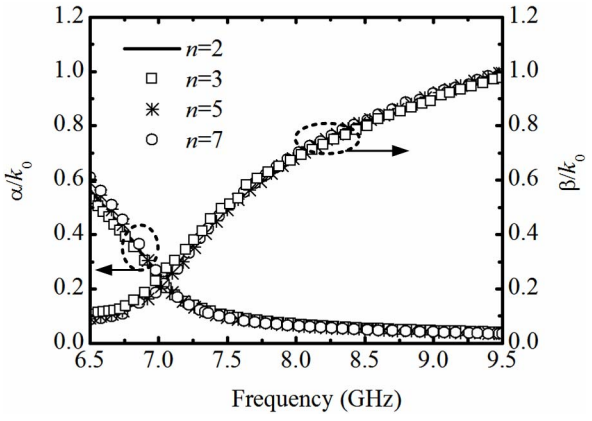

Fig. 5. Numerical convergence on deembedded complex propagation constants with respect to different DUT lengths, $L = nS$. n: vias' number. S: via-to-via spacing. $L_e = 4S$, $w_1 = 6.3$ mm, $S = 1.2$ mm, and the via's diameter is 0.7 mm.

IV. Experiment Verification

The proposed SOC approach is effective and easy to implement for numerical deembedding the guided-wave characteristics of SIW and HMSIW. The main procedures for applying it to calculate the propagation characteristics of SIW or HMSIW are listed as follows.

1) Simulate the entire layout of the two-port SIW or HMSIW network, including two error boxes and

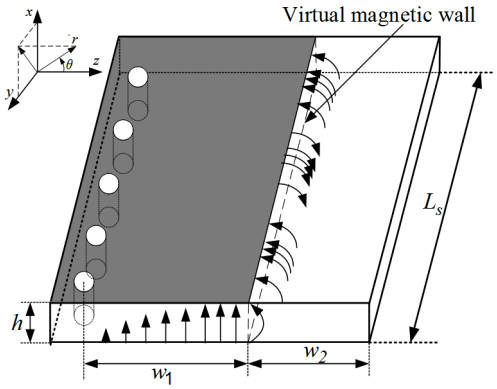

Fig. 6. Electric-field distribution in an HMSIW guided-wave structure.

one core section under deembedding so as to numerically obtain its ABCD matrix [$\boldsymbol{A}$].

2) Calculate the two input impedance Z_{short} and Z_{open} of the error boxes terminated by electric and magnetic walls, respectively.
3) Determine the complex propagation constant of the core SIW or HMSIW with formula (2).

It is worthwhile to note that in order to tradeoff the simulation time and numerical convergence, the length of the error-involved feeding section or error boxes is set a little longer, while the length of the core SIW and HMSIW can be set slightly shorter. The substrate used in this paper is the Taconic TLX with a thickness of 1 mm, relative permittivity of 2.55, and dielectric loss tangent of 0.0019.

A. Example of an HMSIW Leaky Wave Antenna

Fig. 6 shows the 3-D view of HMSIW and its relevant unsymmetrical field distribution. Since the dominant guided-wave mode propagating along the HMSIW is a fast wave, the HMSIW may leak a certain portion of power into the air through the open aperture in its right side [14]. This property may be useful for the construction of a leaky wave antenna. With the use of the above-derived complex propagation constant, its H-plane radiation pattern can be simply and directly calculated as

$$F_\theta = \frac{\sinh((\gamma - jk_0 \sin\theta)L_s/2)}{(\gamma - jk_0 \sin\theta)L_s/2} \cos\theta \tag{3}$$

where k_0 is the free-space phase constant. It is clear that the radiation pattern of the HMSIW leaky wave antenna is primarily determined by its complex propagation constant $\gamma\,(\gamma = \alpha + j\beta)$. In short, the phase constant β determines the main radiation direction, while the attenuation or leakage constant α determines the radiation beamwidth and efficiency.

The effects of a few critical geometrical dimensions on the phase and leakage constants of the HMSIW guided-wave structure for the application in leaky wave antennas were studied with our proposed method. Fig. 7 shows the three sets of normalized complex propagation constant with respect to the dielectric thickness, h. Beyond the cutoff frequency at ~7.3 GHz, the calculated leakage constant is found to shift up while its relevant phase constant gets a certain increment as h increases. It can be intuitively understood that the width

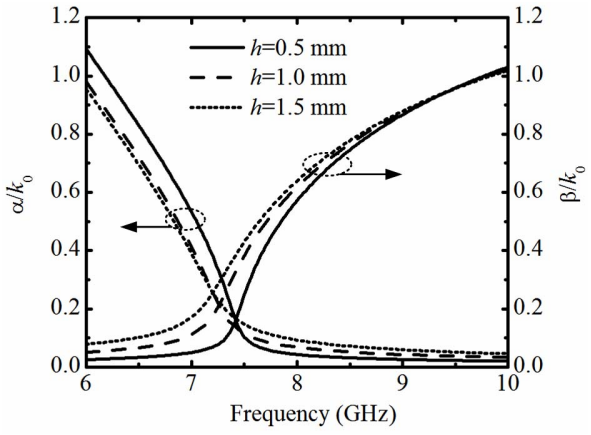

Fig. 7. Complex propagation constants versus dielectric thickness of h.

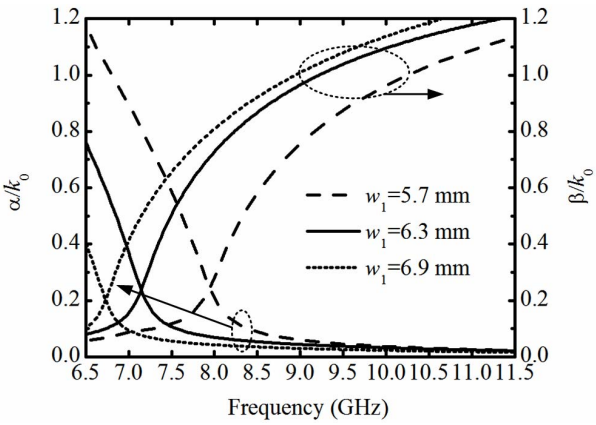

Fig. 8. Complex propagation constants versus top metal width w_1.

Fig. 9. Photography of the fabricated HMSIW leaky-wave antenna and the parameters and coordinate correspond to the ones in Fig. 6. $L_s = 188.4$ mm, $w_2 = 0.2$ mm, $w_1 = 6.3$ mm, $S = 1.2$ mm, and the diameter of via is 0.7 mm.

of the radiation aperture, h, is enlarged and the EM field in the HMSIW disperses itself from the substrate to air.

Fig. 8 shows the normalized complex propagation constants of HMSIW versus a different width of top metal, w_1. It is clearly demonstrated that the cutoff frequency of HMSIW is mainly determined by the value of w_1. With the increase in the value of w_1, the cutoff frequency decreases, and what is more, the leakage constant decreases as well. An HMSIW leaky wave antenna with a small leakage constant usually deteriorates the radiation efficiency, but it can achieve the narrow main radiation beam.

Then, according to the analysis above, an HMSIW leaky wave antenna working at 7.5 GHz is designed. In order to improve the radiation efficiency, the width of the top metal is set as 6.3 mm with an increased leakage constant α. The photograph of fabricated antenna is shown in Fig. 9.

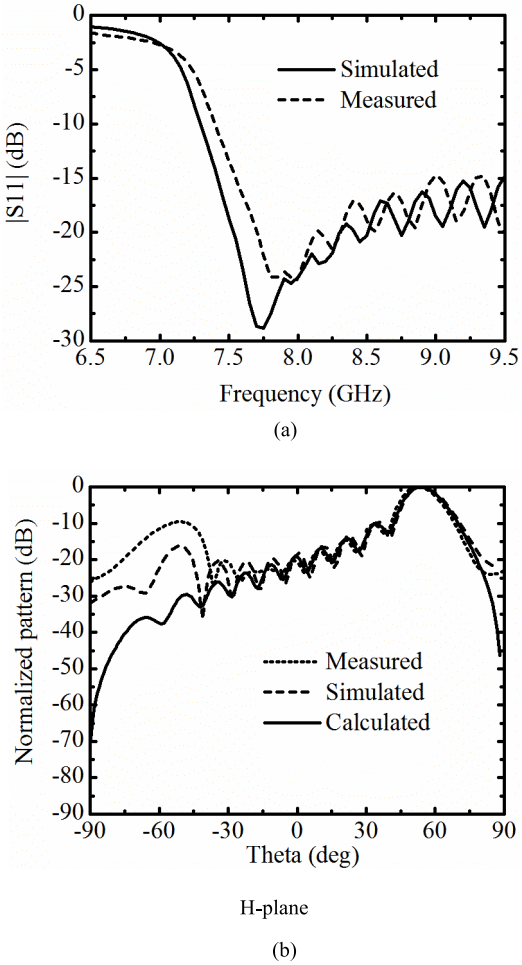

Fig. 10. (a) Simulated and measured reflection coefficients. (b) Calculated, simulated, and measured radiation patterns at 7.5 GHz.

The conventional tapered transitions are introduced at two ports to feed this antenna. The simulated and measured reflection coefficients of the HMSIW leaky wave antenna have been shown in Fig. 10(a), and visible discrepancy between them is mainly caused by the nonideal Sub-Miniature-A (SMA) connectors and fabrication tolerance.

Using (3), the H-plane radiation pattern of this HMSIW leaky wave antenna can be directly calculated, and it is plotted together in Fig. 10(b) with those from the direct simulation and experimental test. The calculated radiation pattern is found to agree well with the simulated and measured ones, especially in the H-plane over a wide angular range around its main beam. The reflection-caused side lobes in the simulated and measured results appear at about $-55°$, and they are mainly caused by the impedance and field mismatches at the loading port of this antenna [32], [33]. Through this design example, the accuracy of the calculated phase and leakage constants deembedded from the presented SOC method has been satisfactorily verified.

B. Example of Microstrip-to-SIW Transitions

A transition is a key element to interface different kinds of components in microwave integrated circuits. Thus, many approaches to design microstrip-to-SIW transitions have been reported in [34]–[38]. To the best of our knowledge, the proposed SIW-based transitions themselves have not yet been well studied as a single transition since the SIW terminals cannot be rigorously defined using EM software as a waveport [16], [17], [25]. As an indirect approach, the reported works only demonstrated the scattering parameters of a so-called back-to-back transition, which is composed of the two single transitions cascaded via an SIW section in the middle. But, this kind of research has not yet really demonstrated the scattering characteristics of a single microstrip-to-SIW transition itself. A method to calculate the scattering parameters of a single SIW-based transition has been given in [16], but the detailed extraction procedures have not been provided. We have presented an approach to numerically deembed the scattering parameters of a single wideband microstip-to-Coplanar waveguide (CPW) transition with virtue to the precalculated complex propagation constant of the CPW in [34]. This method is further developed herein to accurately extract the scattering parameters of a single microstrip-to-SIW transition when the complex propagation constant of the SIW is precalculated using our proposed SOC method.

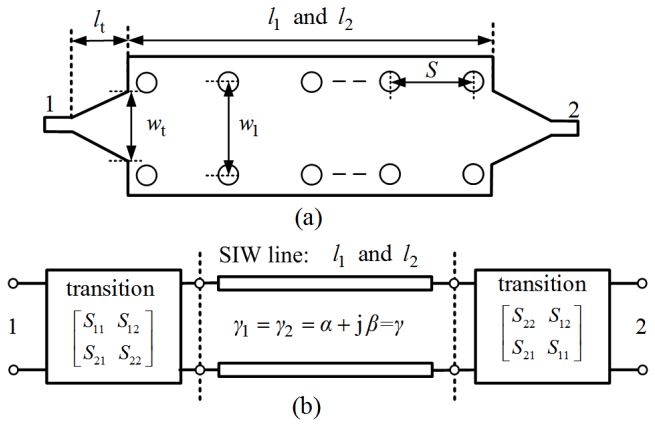

Fig. 11. (a) Model of the classical back-to-back SIW structure with tapered transitions. (b) Equivalent cascaded topology of (a).

As such, the two back-to-back transition structures, as shown in Fig. 11(a), are constructed by cascading the two identical single transitions via the connecting SIW in the middle with two different lengths, i.e., l_1 and l_2. Their respective scattering parameters at the two microstrip feeding lines are represented by $[\boldsymbol{S}^{l_1}]$ and $[\boldsymbol{S}^{l_2}]$, and they are numerically calculated by the EM software. The scattering parameters of a single transition of our concern herein can be explicitly calculated as

$$\begin{aligned} S_{11} &= \frac{S_{11}^{l_1} S_{21}^{l_2} e^{-\gamma l_2} - S_{11}^{l_2} S_{21}^{l_1} e^{-\gamma l_1}}{S_{21}^{l_2} e^{-\gamma l_2} - S_{21}^{l_1} e^{-\gamma l_1}} \\ S_{22} &= \frac{S_{11}^{l_2} - S_{11}^{l_1}}{S_{21}^{l_2} e^{-\gamma l_2} - S_{21}^{l_1} e^{-\gamma l_1}} \\ S_{21}^2 &= \frac{2 S_{21}^{l_2} S_{21}^{l_1} \sinh[\gamma (l_1 - l_2)]}{S_{21}^{l_2} e^{-\gamma l_2} - S_{21}^{l_1} e^{-\gamma l_1}} \end{aligned} \tag{4}$$

where γ stands for the complex propagation constant of the SIW and it consists of the phase and attenuation constants, β and α.

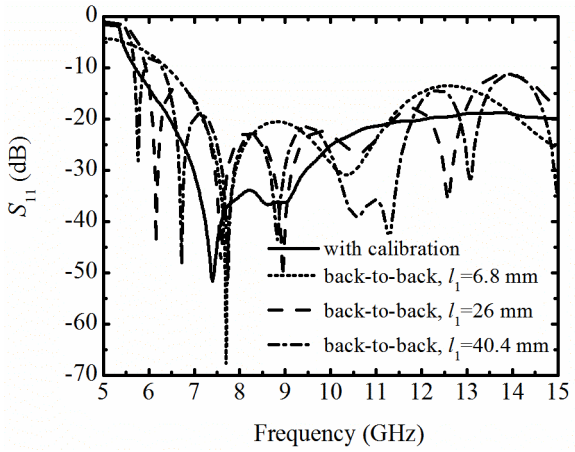

Fig. 12. Comparison of reflection coefficients of single SIW-based transitions between with our calibration method and conventional back-to-back structures. $f_t = 15.6$ mm, $w_t = 7$ mm, $w_1 = 14$ mm, and $S = 2$ mm. The diameter of via is 1 mm. $l_1 = 88.8$ mm and $l_2 = 84$ mm for calibration.

In numerical deembedding procedure, two different lengths of SIW, i.e., l_1 and l_2, should be carefully chosen in order to avoid the numerical singularity at

$$e^{-(\alpha+j\beta)(l_1-l_2)} = S_{21}^{l_2}/S_{21}^{l_1}. \tag{5}$$

Considering the fact that the attenuation constant α is usually very small and its value is very close to zero in the operating frequency bandwidth [17]. In this context, the transmission coefficient $S_{21}^{l_2}$ is almost equal to $S_{21}^{l_1}$ in magnitude regardless of different lengths, l_1 and l_2. Following (4), we can figure out that the two SIW lengths in the middle, l_1 and l_2, should be chosen in the range as defined as

$$0 < |\beta_{\max}(l_1 - l_2)| < \pi \tag{6}$$

where $\beta_{\max}$ is the maximum phase constant of the SIW to be tolerated when (2) is used.

Based on the above-described method, the scattering parameters of a single microstrip-to-SIW transition can be determined in general. Fig. 12 compares the extracted reflection coefficient, S_{11}, of a single tapered transition in Fig. 11(a) and the results obtained from the conventional back-to-back structures. It can be observed that the result of the transition, derived from our numerical calibration, has a wider bandwidth in high frequencies. Moreover, we can see that the reflection coefficients obtained by the conventional methods are tremendously affected by the selected lengths of SIW (l_1) between two transitions.

As another advantage, the proposed method can help us to accurately evaluate the performance of different structures of these SIW-related transitions. As an example, the two typical microstrip-to-SIW transitions, i.e., slot coupling [35] and tapered structures are designed. Based on our proposed SOC method, the complex propagation constant γ of SIW is numerically extracted first. Then, the scattering parameters of a single transition for different structures can be accurately extracted with (4), respectively.

For evident verification, these two transitions are fabricated with their photos shown in Fig. 13. Fig. 14 shows the extracted

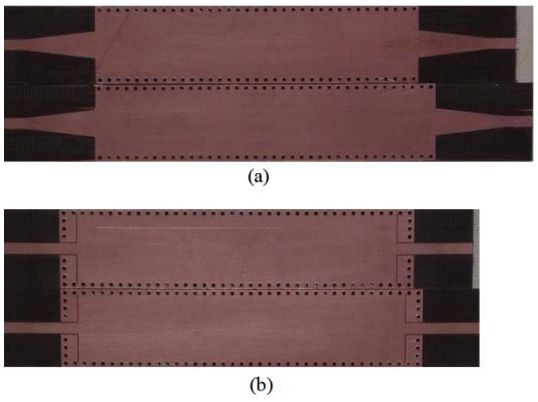

Fig. 13. Photos of two fabricated back-to-back transitions. (a) Microstrip-to-SIW tapered transition ($l_1 = 88.8$, $l_2 = 84$, $f_t = 15.6$, and $w_t = 7$). (b) Slot-coupling transition (slot with/length: 0.2/12, $l_1 = 84.6$, and $l_2 = 82.2$). The other parameters are identical to the ones in Fig. 12 (unit: mm).

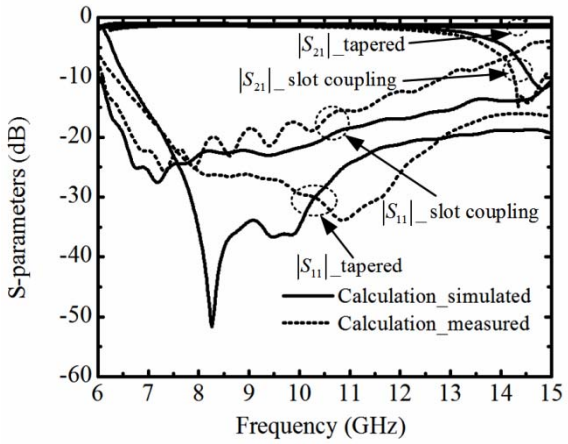

Fig. 14. Extracted scattering parameters from the simulated and measured results of two different structures of SIW-based transitions.

scattering parameters of these single SIW transitions from the simulated and experimented results. It is found that the slot-coupling transition has more compact physical size and better performance near the cutoff frequency, whereas the tapered transition has a wider operating bandwidth up to high frequency. For the slot-coupling transition, the extracted reflection coefficients from the measured and simulated results in Fig. 14 are lower than -15 dB from 6.7 to 12 GHz and slight discrepancy can be observed. The obtained reflection coefficients of the tapered transition show certain disagreement in their shape in Fig. 14, however, both their reflection coefficients have achieved below -20 dB over the 7.3–13.4 GHz and it indicates that the reflected power occupies less than 1% of the incident power. The mentioned visible discrepancies may be mainly attributed to the nonideal SMA connectors in measurement and fabrication tolerance in etching process.

V. Conclusion

In this paper, the conventional SOC has been further extended in the 3-D commercial full-wave software to accurately deembed the complex propagation constants of the SIW and HMSIW. The SOC procedure is described,

and its numerical stability and convergence are confirmed. Two examples are given to apply our proposed method. An HMSIW leaky wave antenna is designed, and its calculated radiation pattern using the deembedded phase and leakage constants is well confirmed in simulation and measurement. Then, the scattering parameters of two classes of single microstrip-to-SIW transitions are studied by our presented extraction approach, and they are both confirmed as well. Experimentally, these two back-to-back microstrip-to-SIW transitions are fabricated and tested to provide evident validation on the predicted frequency response of single microstrip-to-SIW transitions over a wide frequency range. It is our belief that our SOC technique can also be applied to accurately and effectively deembedding of other guided-wave structures with periodically varied geometries.

ACKNOWLEDGMENT

The authors would like to thank Prof. W.-J. Lu, Nanjing University of Posts and Telecommunications, for the valuable suggestions and discussions.

REFERENCES

[1] D. Deslandes and K. Wu, "Integrated microstrip and rectangular waveguide in planar form," *IEEE Microw. Wireless Compon. Lett.*, vol. 11, no. 2, pp. 68–70, Feb. 2001.

[2] M. Bozzi, A. Georgiadis, and K. Wu, "Review of substrate-integrated waveguide circuits and antennas," *IET Microw. Antennas Propag.*, vol. 5, no. 8, pp. 909–920, Jun. 2011.

[3] W. Shen, W.-Y. Yin, X.-W. Sun, and L.-S. Wu, "Substrate-integrated waveguide bandpass filters with planar resonators for system-on-package," *IEEE Trans. Compon., Packag., Manuf. Technol.*, vol. 3, no. 2, pp. 253–261, Feb. 2013.

[4] K.-S. Chin, C.-C. Chang, C.-H. Chen, Z. Guo, D. Wang, and W. Che, "LTCC multilayered substrate-integrated waveguide filter with enhanced frequency selectivity for system-in-package applications," *IEEE Trans. Compon., Packag., Manuf. Technol.*, vol. 4, no. 4, pp. 664–672, Apr. 2014.

[5] S. W. Wong, K. Wang, Z.-N. Chen, and Q.-X. Chu, "Electric coupling structure of substrate integrated waveguide (SIW) for the application of 140-GHz bandpass filter on LTCC," *IEEE Trans. Compon., Packag., Manuf. Technol.*, vol. 4, no. 2, pp. 316–322, Feb. 2015.

[6] S. W. Wong, R. S. Chen, K. Wang, Z.-N. Chen, and Q.-X. Chu, "U-shape slots structure on substrate integrated waveguide for 40-GHz bandpass filter using LTCC technology," *IEEE Trans. Compon., Packag., Manuf. Technol.*, vol. 5, no. 1, pp. 128–134, Jan. 2015.

[7] X.-P. Chen and K. Wu, "Self-packaged millimeter-wave substrate integrated waveguide filter with asymmetric frequency response," *IEEE Trans. Compon., Packag., Manuf. Technol.*, vol. 2, no. 5, pp. 775–782, May 2012.

[8] X. P. Chen, K. Wu, and D. Drolet, "Substrate integrated waveguide filter with improved stopband performance for satellite ground terminal," *IEEE Trans. Microw. Theory Techn.*, vol. 57, no. 3, pp. 674–683, Mar. 2009.

[9] L.-S. Wu, Y.-X. Guo, J.-F. Mao, and W.-Y. Yin, "Design of a substrate integrated waveguide balun filter based on three-port coupled-resonator circuit model," *IEEE Microw. Wireless Compon. Lett.*, vol. 21, no. 5, pp. 252–254, May 2011.

[10] B. Liu, W. Hong, Y.-Q. Wang, Q.-H. Lai, and K. Wu, "Half mode substrate integrated waveguide (HMSIW) 3-dB coupler," *IEEE Microw. Wireless Compon. Lett.*, vol. 17, no. 1, pp. 22–24, Jan. 2007.

[11] T. Djerafi, D. Hammou, K. Wu, and S. O. Tatu, "Ring-shaped substrate integrated waveguide Wilkinson power dividers/combiners," *IEEE Trans. Compon., Packag., Manuf. Technol.*, vol. 4, no. 9, pp. 1461–1469, Sep. 2014.

[12] H. Wong, Q. W. Lin, H. W. Lai, and X. Y. Zhang, "Substrate integrated meandering probe-fed patch antennas for wideband wireless devices," *IEEE Trans. Compon., Packag., Manuf. Technol.*, vol. 5, no. 3, pp. 381–388, Mar. 2015.

[13] C. Jin, R. Li, S. Hu, S. Zhang, K. F. Chang, and B. Zheng, "Self-shielded circularly polarized antenna-in-package based on quarter mode substrate integrated waveguide subarray," *IEEE Trans. Compon., Packag., Manuf. Technol.*, vol. 4, no. 3, pp. 392–399, Mar. 2014.

[14] J. Liu, D. R. Jackson, Y. Li, C. Zhang, and Y. Long, "Investigations of SIW leaky-wave antenna for endfire-radiation with narrow beam and sidelobe suppression," *IEEE Trans. Antennas Propag.*, vol. 62, no. 9, pp. 4489–4497, Sep. 2014.

[15] A. Mallahzadeh and S. Mohammad-Ali-Nezhad, "Long slot ridged SIW leaky wave antenna design using transverse equivalent technique," *IEEE Trans. Antennas Propag.*, vol. 62, no. 11, pp. 5445–5452, Nov. 2014.

[16] S. Georgakopoulos and S. Ogurtsov, "An S-parameter extraction technique for broad-band characterization of microstrip-to-SIW transitions," in *Proc. IEEE Antennas Propag. Soc. Int. Symp.*, Jun. 2009, pp. 1–4.

[17] F. Xu and K. Wu, "Guided-wave and leakage characteristics of substrate integrated waveguide," *IEEE Trans. Microw. Theory Techn.*, vol. 53, no. 1, pp. 66–73, Jan. 2005.

[18] B. Y. El Khatib, T. Djerafi, and K. Wu, "Substrate-integrated waveguide vertical interconnects for 3-D integrated circuits," *IEEE Trans. Compon., Packag., Manuf. Technol.*, vol. 2, no. 9, pp. 1526–1535, Sep. 2012.

[19] B. Bensalem and J. T. Aberle, "A new high-speed memory interconnect architecture using microwave interconnects and multicarrier signaling," *IEEE Trans. Compon., Packag., Manuf. Technol.*, vol. 4, no. 2, pp. 332–340, Feb. 2014.

[20] J. Liu, Y. Li, S. Zheng, and Y. Long, "Method of auxiliary sources for analyzing half-mode substrate integrated waveguide," *IEEE Antennas Wireless Propag. Lett.*, vol. 13, pp. 1043–1046, Jun. 2014.

[21] F. Xu, K. Wu, and W. Hong, "Domain decomposition FDTD algorithm combined with numerical TL calibration technique and its application in parameter extraction of substrate integrated circuits," *IEEE Trans. Microw. Theory Techn.*, vol. 54, no. 1, pp. 329–338, Jan. 2006.

[22] Y. Cassivi, L. Perregrini, P. Arcioni, M. Bressan, K. Wu, and G. Conciauro, "Dispersion characteristics of substrate integrated rectangular waveguide," *IEEE Microw. Wireless Compon. Lett.*, vol. 12, no. 9, pp. 333–335, Sep. 2002.

[23] M. Salehi and E. Mehrshahi, "A closed-form formula for dispersion characteristics of fundamental SIW mode," *IEEE Microw. Wireless Compon. Lett.*, vol. 21, no. 1, pp. 4–6, Jan. 2011.

[24] Q. Lai, C. Fumeaux, W. Hong, and R. Vahldieck, "Characterization of the propagation properties of the half-mode substrate integrated waveguide," *IEEE Trans. Microw. Theory Techn.*, vol. 57, no. 8, pp. 1996–2004, Aug. 2009.

[25] L. Zhu and K. Wu, "Unified equivalent-circuit model of planar discontinuities suitable for field theory-based CAD and optimization of M(H)MIC's," *IEEE Trans. Microw. Theory Techn.*, vol. 47, no. 9, pp. 1589–1602, Sep. 1999.

[26] L. Li, K. Wu, and L. Zhu, "Numerical TRL calibration technique for parameter extraction of planar integrated discontinuities in a deterministic MoM algorithm," *IEEE Microw. Wireless Compon. Lett.*, vol. 12, no. 12, pp. 485–487, Dec. 2002.

[27] L. Li and K. Wu, "Numerical through-resistor (TR) calibration technique for modeling of microwave integrated circuits," *IEEE Microw. Wireless Compon. Lett.*, vol. 14, no. 4, pp. 139–141, Apr. 2004.

[28] L. Li and K. Wu, "Multiport through-resistor (TR) numerical calibration," *IEEE Microw. Wireless Compon. Lett.*, vol. 15, no. 12, pp. 883–885, Dec. 2005.

[29] X.-P. Chen and K. Wu, "Accurate and efficient design approach of substrate integrated waveguide filter using numerical TRL calibration technique," in *IEEE MTT-S Int. Microw. Symp. Dig.*, Jun. 2008, pp. 1231–1234.

[30] F. Xu, K. Wu, and X. Zhang, "Periodic leaky-wave antenna for millimeter wave applications based on substrate integrated waveguide," *IEEE Trans. Antennas Propag.*, vol. 58, no. 2, pp. 340–347, Feb. 2010.

[31] R. B. Marks, "A multiline method of network analyzer calibration," *IEEE Trans. Microw. Theory Techn.*, vol. 39, no. 7, pp. 1205–1215, Jul. 1991.

[32] C. J. Wang, J. J. Wu, C. C. Hu, and C. F. Jou, "Asymmetric feeding active leaky-wave antenna arrays," *Microw. Opt. Technol. Lett.*, vol. 18, no. 1, pp. 14–17, May 1998.

[33] A. J. Martinez-Ros, J. L. Gomez-tornero, and G. Goussetis, "Conformal tapered substrate integrated waveguide leaky-wave antenna," *IEEE Trans. Antennas Propag.*, vol. 62, no. 12, pp. 5983–5991, Dec. 2014.

[34] L. Zhu and W. Menzel, "Broad-band microstrip-to-CPW transition via frequency-dependent electromagnetic coupling," *IEEE Trans. Microw. Theory Techn.*, vol. 52, no. 5, pp. 1517–1522, May 2004.

[35] R.-Y. Fang, C.-F. Liu, and C.-L. Wang, "Compact and broadband CB-CPW-to-SIW transition using stepped-impedance resonator with 90°-bent slot," *IEEE Trans. Compon., Packag., Manuf. Technol.*, vol. 3, no. 2, pp. 247–252, Feb. 2013.
[36] N. Ghassemi, I. Boudreau, D. Deslandes, and K. Wu, "Millimeter-wave broadband transition of substrate integrated waveguide on high-to-low dielectric constant substrates," *IEEE Trans. Compon., Packag., Manuf. Technol.*, vol. 3, no. 10, pp. 1764–1770, Oct. 2013.
[37] Z. Kordiboroujeni and J. Bornemann, "New wideband transition from microstrip line to substrate integrated waveguide," *IEEE Trans. Microw. Theory Techn.*, vol. 62, no. 12, pp. 2983–2989, Dec. 2014.
[38] D. Deslandes and K. Wu, "Analysis and design of current probe transition from grounded coplanar to substrate integrated rectangular waveguides," *IEEE Trans. Microw. Theory Techn.*, vol. 53, no. 8, pp. 2487–2494, Aug. 2005.

Zheng Liu (S'12) was born in Shandong, China, in 1984. He is currently pursuing the Ph.D. degree with Shanghai Jiao Tong University, Shanghai, China.

He was an Exchange Student with the University of Macau, Macau, China, from 2014 to 2015. His current research interests include microwave and millimeter-wave passive and active components and circuits.

Lei Zhu (S'91–M'93–SM'00–F'12) received the B.Eng. and M.Eng. degrees in radio engineering from Southeast University, Nanjing, China, in 1985 and 1988, respectively, and the Ph.D. degree in electronics engineering from the University of Electro-Communications, Tokyo, Japan, in 1993.

He was a Research Engineer with Matsushita-Kotobuki Electronics Industries Ltd., Tokyo, from 1993 to 1996. From 1996 to 2000, he was a Research Fellow with the École Polytechnique de Montréal, Montréal, QC, Canada. From 2000 to 2013, he was an Associate Professor with the School of Electrical and Electronic Engineering, Nanyang Technological University, Singapore. Since 2013, he has been a Professor with the Faculty of Science and Technology, University of Macau, Macau, China. Since 2014, he has served as the Head of the Department of Electrical and Computer Engineering with the University of Macau. He has authored or co-authored over 275 papers in peer-reviewed journals and conference proceedings. His papers have been cited more than 3370 times with an h-index of 32 according to ISI Web of Science. His current research interests include microwave circuits, guided-wave periodic structures, antennas, and computational electromagnetic techniques.

Prof. Zhu was a recipient of the 1997 Asia-Pacific Microwave Prize Award, the 1996 Silver Award of Excellent Invention from Matsushita-Kotobuki Electronics Industries Ltd., and the 1993 First-Order Achievement Award in Science and Technology from the National Education Committee, China. He was an Associate Editor of the IEEE TRANSACTIONS ON MICROWAVE THEORY AND TECHNIQUES from 2010 to 2013, and the IEEE MICROWAVE AND WIRELESS COMPONENTS LETTERS from 2006 to 2012. He served as the General Chair of the 2008 IEEE MTT-S International Microwave Workshop Series on the Art of Miniaturizing RF and Microwave Passive Components, Chengdu, China, and the Technical Program Committee Co-Chair of the 2009 Asia-Pacific Microwave Conference, Singapore. He has served as a member of the IEEE MTT-S Fellow Evaluation Committee and the IEEE AP-S Fellows Committee since 2013 and 2015, respectively.

Gaobiao Xiao (M'02) received the M.S. degree from the Huazhong University of Science and Technology, Wuhan, China, in 1988, the B.S. degree from the National University of Defense Technology, Changsha, China, in 1991, and the Ph.D. degree from Chiba University, Chiba, Japan, in 2002.

He was with Hunan University, Changsha, from 1991 to 1997. Since 2004, he has been a Faculty Member with the Department of Electronic Engineering, Shanghai Jiao Tong University, Shanghai, China. His current research interests include numerical methods in electromagnetic fields, coupled thermoelectromagnetic analysis, microwave filter designs, fiber-optic filter designs, and inverse scattering problems.

Qiong Sen Wu was born in Maoming, China, in 1989. He received the B.S. and M.E. degrees from the South China University of Technology, Guangzhou, China, in 2011 and 2014, respectively. He is currently pursuing the Ph.D. degree with the University of Macau, Macau, China.

His current research interests include millimeter-wave power-combining circuits, periodic guided-wave structures, and impedance transformers.